Organic & Biomolecular Chemistry

Accepted Manuscript

ROYAL SOCIETY OF CHEMISTRY

www.rsc.org/obc

D-isonucleoside (isoNA) incorporation around cleavage site of passenger strand promotes the vibration of Ago2-PAZ domain and enhances in vitro potency of siRNA

[#]Ye Huang,[a,e] [#]Miao Tian,[a] Yichao Zhang,[c] Gang Sheng,[b] Zhuo Chen,[a] Yuan Ma,[a] Yue Chen,[a] Yihong Peng,[d] Yilei Zhao,*[c] Yanli Wang,[b] Lihe Zhang[a] and Zhenjun Yang*[a]

[#]These authors contributed equally to this paper

a. State Key Laboratory of Natural and Biomimetic Drugs, School of Pharmaceutical Sciences, Peking University, Beijing, 100191, China. Email: yangzj@bjmu.edu.cn

b. Laboratory of Non-Coding RNA, Institute of Biophysics, Chinese Academy of Sciences, Beijing, China.

c. State Key Laboratory of Microbial Metabolism, School of Life Sciences and Biotechnology, Shanghai Jiao Tong University, Shanghai, China. Email: yileizhao@sjtu.edu.cn

d. Department of Microbiology, School of Basic Medical Sciences, Peking University, Beijing, China

e. *Department of New Drug Research and Development, Institute of Materia Medica, Peking Union Medical College & Chinese Academy of Medical Sciences, Beijing, China.*

It has been demonstrated that passenger strand cleavage is important for RNA-induced silencing complex (RISC) activation, which is crucial step for siRNA-mediated gene silencing. Here, we reported that isonucleotide (isoNA) modification around cleavage site of passenger strand would affect in vitro potency of modified siRNAs by altering the motion pattern of Ago2-PAZ domain. According to western blotting, q-PCR and antiviral results, we proved that D-isonucleotide (isoNA) modification at position 8 of passenger strand (siMek1-S08D), where is adjacent to cleavage site, improved in vitro potency of modified siRNA obviously. While siRNAs with D-isoNA incorporation at position 9 (siMek1-S09D) or L-isoNA incorporation at position 8 and 9 (siMek1-S08L, siMek1-S09L) all showed lower activity compared to native siRNA. The kinetics evaluation of passenger strand cleavage induced by *T. thermophilus* Ago (Tt-Ago) showed that D-isoNA modification at position 8 of passenger strand had no remarkable influence on cleavage rate, but L-isoNA modification at position 8 slowed cleavage rate obviously. And results of molecular dynamics simulation showed that D-isoNA modification at position 8 affected the open-close motion of PAZ domain in Ago/siRNA complex, which may promote the RISC loading and the release of passenger strand cleavage product, and consequently accelerate the RISC activation and enhance the silencing activity. But D-isoNA modification at position 9 or L-isoNA at position 8 or 9 all presented quite opposite influences on the motion of Ago-PAZ domain.

Introduction

Since the discovery of RNA interference (RNAi) effect in *Caenorhabditis elegans*,[1] double-stranded small interfering RNA (siRNA) molecules have been proved to be able to take potent gene knock-down effect in mammalian cells[2] and other eukaryotes.[3-5] The assembly of RNA-induced silencing complex (RISC) is the pivotal step in RNAi pathway.[6] In humans, siRNA duplex with both guide strand and passenger strand is first recognized by RLC complex containing Dicer and the RNA-binding protein TRBP to form immature RISC complex.[7] Then the passenger strand was nicked between position 9 and 10 counted form 5'-termianl by Argonaute 2 (Ago2) protein in the same way as target mRNA being cleaved,[8,9] followed by being degraded by C3PO to finally activate the RISC.[10] The active RISC recognize and cleavage the complementary target RNA to execute the silencing process.

Dramatic reduction in the cleavage efficiency of target RNA was found when chemical modification happened around the nicked site of passenger strand. These chemical modifications may limit the formation of RISC and then impaired silencing activity of siRNA by blocking the cleavage of passenger strand.[8,11] For example, replacing the phosphodiester linkage between position 9 and position 10 with phosphorothioate, modifying position 9 with a 2'-O-methyl ribose, introducing 4-nt mismatches from position 9 to position 11, all caused great reduction in the cleavage efficiency of the complementary target RNA. However, the same modifications positioned 1 or 2nt downstream of the cleavage site or away from the central position did not affect target RNA cleavage.[11] On the other side, when thermally destabilizing modifications were placed around cleavage site of passenger strand, obvious enhancement of silencing activity was found.[12] This unusual phenomenon may be owing to that thermally destabilizing modifications loose the regional conformation around the activity site and promote the cleavage related residues of Ago2 protein to interact with the phosphodiester bond between position 9 and position 10 of passenger strand. All these reports indicated that conformation alteration around cleavage site of passenger strand may affect the silencing activity.

Isonucleoside (isoNA) (**Figure 1A**) is a novel type of nucleoside analogue in which the nucleobase is moved to another position of ribose other than C-1'.[13,14] In our previous work, we found that isonucleotide modification could alter regional conformation around incorporation site when modified DNA or RNA oligonucleotides were hybridized with complementary DNA/RNA strand. For example, L-isoNA modificaition at the 3'-terminus of DNA oligonucleotides conferred a conformation blocking exonuclease recognition and then increased their exonuclease resistant ability; whereas L-isoNA modification in the middle of oligonucleotides altered the regional conformation into the form that is more suitable for RNase H recognition and then enhanced the degradation of the complementary RNA.[15-17] Then we reported that D-isoNA and L-isoNA incorporation could introduce regional conformation alteration into siRNA duplex and affect the physicochemical and biological properties at varying degrees.[18] Therefore, D-/L-isoNA could be applied as a pair of chemical tools to explore the systematic relationship between the conformational alteration around every single nucleotide of siRNA and their biological potency.

Through the thermal denaturation and dynamic simulation studies, we have demonstrated that D-isoNA and L-isoNA modification at position 8 and 9 of passenger strand would affect the original compacted duplex by introducing flexible conformation of different degrees.[18] Therefore, in this paper, further silencing activity, antivirus activity and dynamic

simulation studies were applied to deeply explore the influence of regional conformation alteration caused by D-/L-isoNA modification on the process of passenger strand cleavage and the silencing potency of modified siRNAs. The siRNA sequence targeting the MEK1 kinase mRNA, which was crucial for the replication process of various usual viruses, was chosen for further silencing activity and anti-virus activity evaluation *in vitro* (**Figure 1B**).[19,20]

Results

Silencing activity affected by D-/L-isoNA incorporation at position 8 and 9 of passenger strand

Quantitative PCR and Western blotting were utilized to investigate silencing activity of the synthesized siRNAs with D-/L-isoNA modification at passenger strand at RNA level and protein level, respectively, in HEK293 cell line. According to results of qPCR evaluation, when position 8 on passenger strand was replaced with D-isoNA (siMek1-S08D), a more potent silencing potency than the native one was found, in contrary, L-isoNA at the same position 8 (siMek1-S08L) impaired the silencing potency. But at the position 9, both D-isoNA and L-isoNA showed decreased silencing activity, however, the difference between unmodified and modified siRNAs was not as obvious as siMek1-S08L (**Figure 1C**). This same phenomenon was also found at protein level that S08D exhibited the strongest knock down effect, while S08L was worse than the native one. D-/L-isoU modification at position 9 showed decreased silencing activity compared to native one either and the difference was more obvious at protein level (**Figure 1D**). The difference between the silencing activity of siMek1-S08D, siMek1-S08L and the native siMek1 were nearly the same at three different concentrations of siRNAs, 5 nM, 10 nM, 30 nM. It indicated that siMek1-S08D provided the best silencing activity regardless of the concentration, although the degree of enhancement was not obvious when the concentration of siRNAs was too low, such as at 5 nM (**Figure 1E**). In a word, D-IsoNA modification at position 8 of passenger strand was able to enhance the in vitro potency of siRNA.

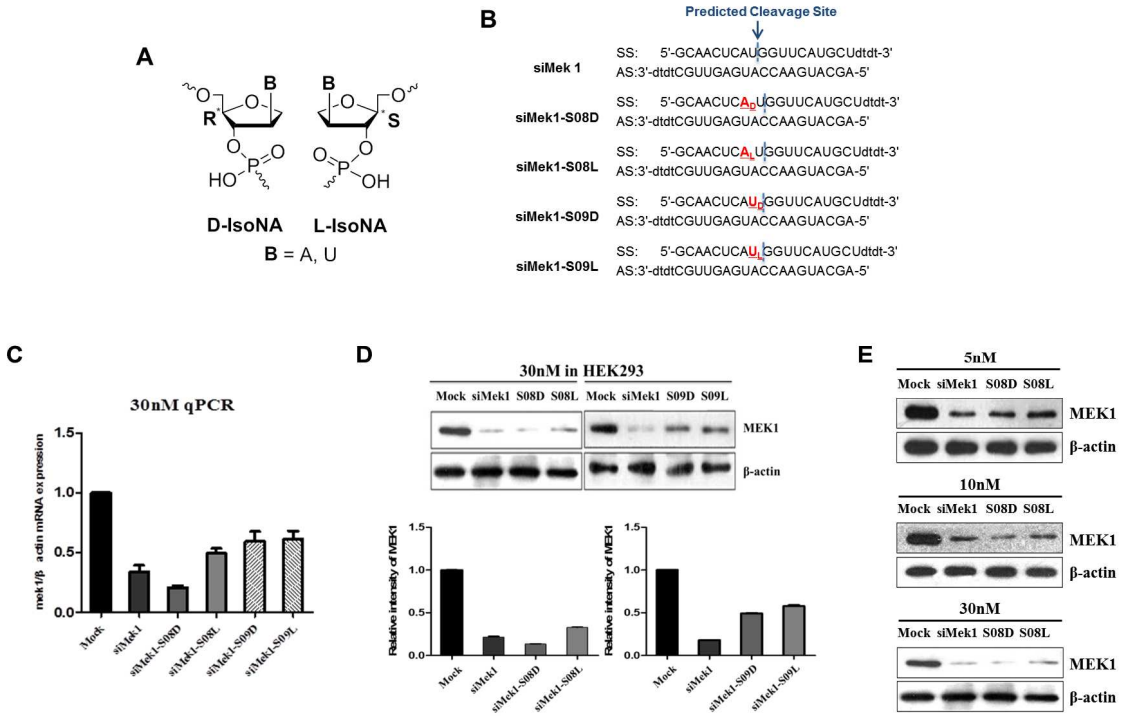

Figure 1. Silencing activity affected by D-/L-isoNA modification at position 8 and 9 of passenger strand. (A) Structures of D-isonucleotide (D-IsoNA, left) and L-isonucleotide (L-IsoNA, right). (B) Sequences of siMek1s modified with D-IsoNA or L-IsoNA at passenger strand. The blue dotted lines represent the predicted cleavage site. (C) Quantitative PCR results of mek1 mRNA. HEK293 cells were co-transfected with siMek1 and siMek1s modified with D-isoNA or L-isoNA at passenger strand at 30 nM of each. Mek1 mRNA was measured 24 h later by quantitative PCR. The mek1 mRNA levels were normalized to β-actin mRNA which was used as a loading control. The uninhibited normalized mek1 mRNA level was set to 100%. The data were the average of three independent experiments and error bars denoted the standard deviations. (D) Western blotting analysis of MEK1 protein. HEK293 cells were co-transfected with siMek1 and siMek1s modified with D-isoNA or L-isoNA at passenger strand at 30 nM of each. Protein lysates were prepared at 36h and blotted with MEK1 antibodies. Quantification of mek1 bands were normalized by densitometric scanning of actin using the band leader software (version

3.0). The relative intensity of MEK1 on y-axis was presented by percentage of intensity of mock transfection (100%). The data were the average of three independent experiments and error bars denoted the standard deviations. (E) Western blotting analysis of MEK1 protein when HEK293 cells were co-transfected with siRNAs at 5 nM, 10 nM, 30 nM, respectively.

Influence of isoNA modification on the kinetics of passenger strand cleavage induced by *T. thermophilus* Ago (Tt-Ago)

According to the results of silencing activity evaluation, D-isoNA modification at position 8 of passenger strand may improve the silencing effect of siRNA. Conversely, other modification strategies around this area, such as L-isoNA at the same position or D-/L-at the adjacent position 9, would impair the activity. In previous reports, those chemical modifications which disturb the cleavage of passenger strand were found to be able to impair silencing activity of siRNA by limiting the formation of RISC.[11] It reminds us that IsoNA modification around the cleavage site of passenger strand may also modulate the silencing activity by affecting the efficiency of cleavage process or other steps directly. Therefore, the influence on kinetics of passenger strand cleavage induced by *T. thermophilus* Ago (Tt-Ago) caused by isoNA modification was evaluated. Previous reports studied the cleavage kinetics of passenger strand with 5'-^{32}P-radiolabeled RNA oligonucleotide.[11] They detected the cleavage fragment of passenger strand via imaging the autoradiography of ^{32}P. However, the labelling process of ^{32}P is complicated, time-consuming and dangerous. Here, we detected the cleavage fragment with 3'-terminal Cy3 labelled passenger RNA instead of 5'-^{32}P-radiolabeled RNA oligonucleotide. In order to avoid the influence on RISC activation caused by steric hindrance of Cy3 group, four extra uridine nucleotides were added at the 3'-terminus (**Figure 2A**).

According to the results of cleavage kinetics (**Figure 2B**), when D-isoNA and L-isoNA were incorporated at position 8 and 9 of passenger strand, none of them disturbed the cleavage process dramatically. The cleavage of all the five 3'-Cy3 labelled RNA strands, Cy3-MKS-23, Cy3-MKS-2308D, Cy3-MKS-2308L, Cy3-MKS-2309D, Cy3-MKS-2309L were started after 30 min and finished after 120 min. However, according to the fluorescence intensity at 60 min, we found that D-isoNA modification affected the cleavage process less than L-isoNA modification. That Cy3-MKS-2308D, Cy3-MKS-2309D had nearly the same cleavage rate as Cy3-MKS-23, but the cleavage of Cy3-MKS-2308L, Cy3-MKS-2309L was slower. It indicated that the low silencing activity of S08L, S09L may be owing to the disturbance caused by L-isoNA incorporation on the interaction between the PIWI domain of Ago and the cleavage site of passenger RNA. Above all, the stronger silencing activity of S08D could not be simply explained through the cleavage kinetics experiment.

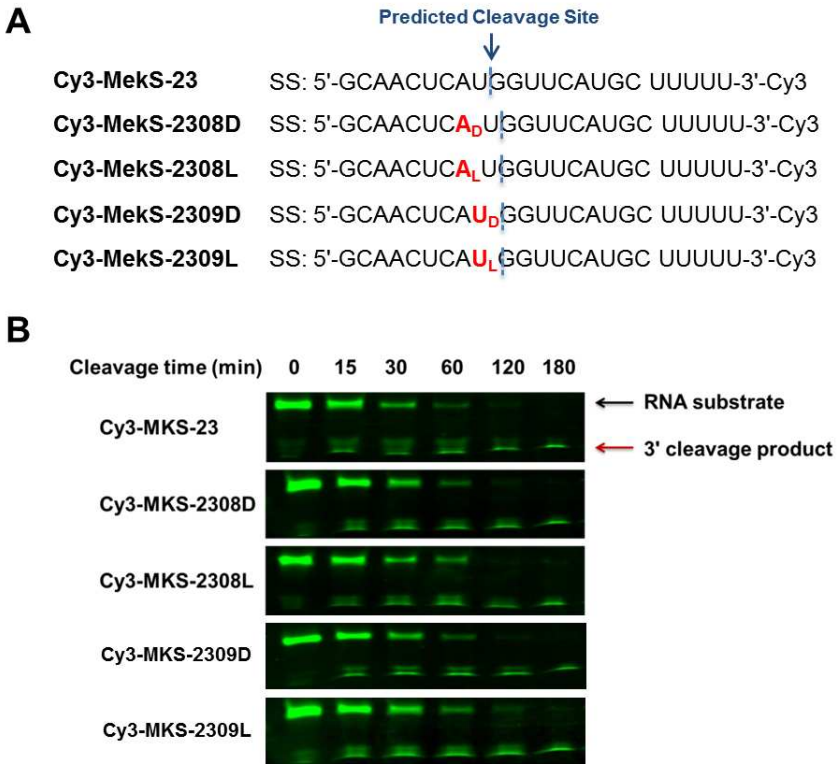

Figure 2. Influence of isoNA modification on the kinetics of passenger strand cleavage induced by *T. thermophilus* Ago (Tt-Ago). (A) Sequences of 3'-Cy3 labeled D-/L-isoNA modified siRNA. (B) The kinetics of passenger strand cleavage induced by *T. thermophilus* Ago (Tt-Ago). Reaction buffer: 10 mM Hepes (pH=7.5), 100 mM NaCl, 5 mM $MnCl_2$; 5 μM Tt-Ago and 5

μM guide DNA strand, incubation in 42 °C for 30 min; then 3 μM passenger RNA strand was added, and incubation temperature raised to 70 °C for cleavage reaction; the cleavage mixture were sampled at 0 min, 15 min, 30 min, 60 min, 120 min, 180 min, respectively and being separated on a 20% PAGE gel with cleavage fragment visualized under fluorescent lights. Black arrow points at the intact passenger RNA substrate and red arrow points at 3'-cleavage passenger RNA fragment.

Stability of the Ago/siRNA complexes and motion change of Ago functional domains

Then the mechanism for this difference was explored by molecular dynamic simulation. The RMSF of the five simulation models of complex with Ago2 and siRNAs are show in **Figure 3A**. In Ago_Native model with no modification, there are two loops that are obviously flexible. As shown in **Figure 3B**, the two loops belong to two different functional domains, PAZ and PIWI, and the PAZ loop is more flexible than the PIWI loop. After isoNA modifications, the flexibility of the two loops decreased especially for the PAZ loop. Ago_S08D model has the least decrease while Ago_S08L has the largest decrease. For siRNA part, there is no detectable change of flexibility.

The four different domains of Ago protein play crucial functions in the cleavage process respectively. We have found that the flexibility of PAZ and PIWI domains changed after isoNA modification, but there is no idea how the motions of the domains vary. Principle Component Analysis (PCA) is performed to the Ago/siRNA models so as to reveal the significant transformation of the functional domains. From the PC1 in Ago_Native model (**Figure 3D**), we found an obvious open-close motion for the PAZ loop, which is in according with the RMSF result and also found in other molecular dynamics simulation. The open-close motion of PAZ loop is thought to be important for the propagation of the guide and target strand and tends to be significantly different depending on whether target strand participates or not. It is conceived that the open-close motion of the PAZ loop is essential for the uptake of siRNA duplex, propagation of the guide and target strand and maybe also determine the release of passenger strand cleavage products. For Ago_S08D model, similar motions are found in PC2 and PC3, which means the PAZ loop behaves at a higher frequency. To ensure the open-close motion, we check the distance between the most flexible residue in the PAZ loop and the active site. The open-close ranges vary from 30Å to 57Å along this indicator (**Figure 3C**) for the Ago_Native model. Similar motion is also observed for Ago_S08D model but with a slightly small cycle. The other three models don't behave similar motions and the distances change little. On the other side, there is no obvious motion for the PIWI loop around 490 which has high RMSF, it means that they behave randomly.

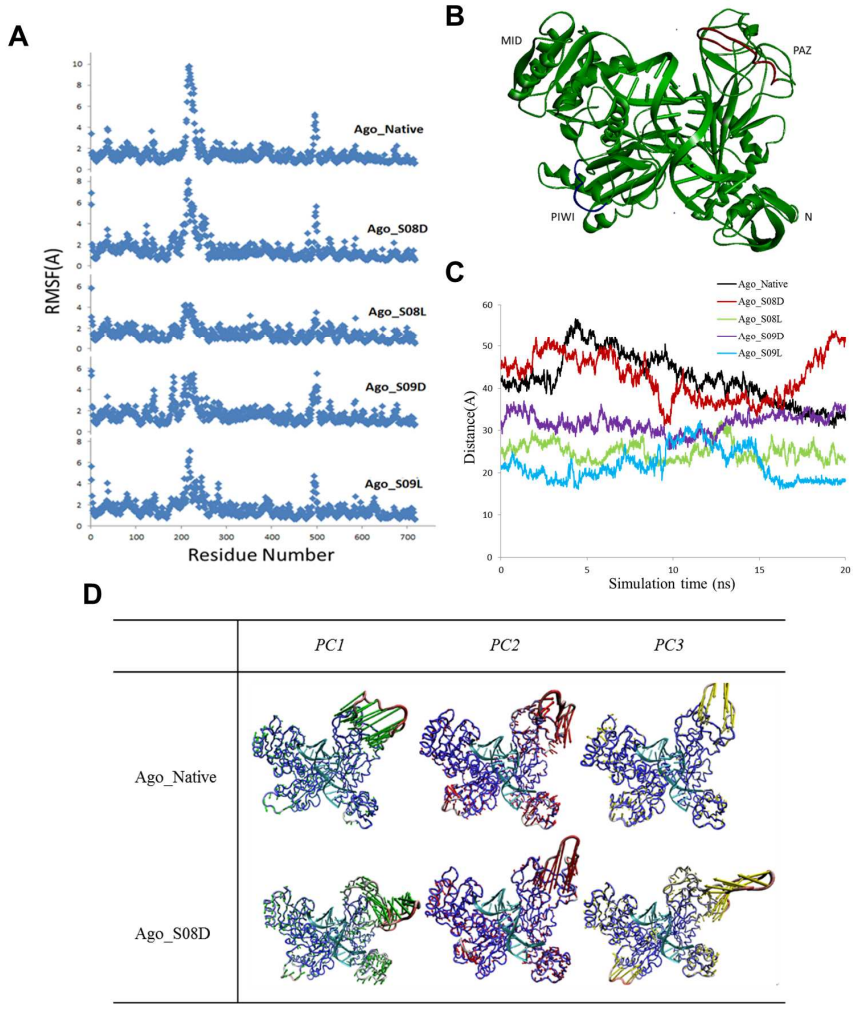

Figure 3. Stability of the Ago/siRNA complexes. (A) The RMSF of each residue in the Ago/siRNA complexes for the last 20ns; (B) The Ago/siRNA complex of Ago_Native model. The red loop refers to the first RMSF peak that appears around residue 220, the blue loop refers to the second RMSF peak that appears around residue 490; (C) The distances between the most flexible residue and the active site of each model during the simulation; (D) The first three principal components (PCs) of Ago_Native and Ago_S08D models during the simulation period.

Binding affinity change after isoNA modifications

Binding free energy of RISC/ssRNA indicates the release obstacle of product after the cleavage of the passenger strand. After the isoNA modifications, the binding free energy deceases in term of Ago_S08D while those of the other three modifications (Ago_S08L, Ago_S09D and Ago_S09L) increase (**Table 1**). The activation of RISC may become easier for Ago_S08D owing to the easier of passenger strand discarded, while the other three isoNA modification strategies prevent the formation of active RISC. The difference may be related to the motion of PAZ loop where the channel with S08D involved closed more than native complex (**Figure 3**) and then inhibit the interaction between S08D with Ago2 protein.

Table 1. The binding free energies of Ago/siRNA and RISC/ssRNA for each of the models (kcal/mol)

	Ago/siRNA	RISC/ssRNA
Ago_Native	-587.7944 ± 25.5832	-254.2087 ± 20.9272
Ago_S08D	-567.7166 ± 24.0868	-246.0320 ± 17.8012
Ago_S08L	-603.6906 ± 32.4930	-282.1824 ± 24.5516
Ago_S09D	-610.9651 ± 22.4295	-277.2535 ± 15.9013

Ago_S09L	-598.7532 ± 25.6560	-278.9986 ± 19.8106

Anti-viral effects of D-/L-isoNA incorporation at position 8 of passenger strand

Then the difference between silencing activity of 8D and 8L were further explored in downstream antivirus effect. Human herpes simplex virus type 2 (HSV2) belongs to the alpha herpesvirus subfamily, and infection with HSV2 produces strong morbidity and shows broad prevalence, long latency, and difficult curability. To date, no preventive vaccines or effective therapeutic drugs for recurrent infections are available.[21] Enterovirus 71 (EV71) is a positive single stranded RNA virus belonging to the family of Picornaviridae, which is known to manifest hand-foot-and mouth disease (HFMD) in young children, and can lead to the development of severe neurological diseases in some patients especially children. By now the treatment and control of EV71 infection are only symptomatic due to the lack of effective medications and unavailability of a prophylactic vaccine.[22] The inhibition of MEK has been studied as the most effective way of investigating the importance of the MAPK cascade in various cellular physiological and pathological processes, including HSV2 and EV71 infection. Here we studied the anti-HSV2 and anti-EV71 effects of siMek1 with D/L-IsoA modification at position 8 of passenger strand by western blotting, virus titration and morphological analysis. To further determine the anti-viral effect of modified siMek1s on ERK activation by HSV-2 or EV71, HEK 293 cells or RD cells were transfected with siRNAs respectively, and then infected with HSV-2 or EV71. As shown in **Figure 4A** and **Figure 4B** siMek1s effectively silenced the expression of MEK1 and viral-gB protein. Furthermore, in consist with the former results, S08D has better effect than the native and S08L on anti-viral effects either.

As one of the most important index of the viral replication, viral titer reflects the release of the live virus in the supernatant of cells infected with the virus. To investigate the influence of D-/L-isoNA modified siRNAs in HSV2 replication, HEK293 cells transfected with siMek1s were infected with HSV-2 and RD cells with EV71, compared with control cells infected with HSV-2 or EV71 alone, and then the virus production was examined. As shown in **Figure 4C**, in the cells transfected with 30 nM siRNAs, HSV2 titers were markedly inhibited, as compared to control cells infected with HSV-2 or EV71 alone. Although not obviously as HSV2, the EV71 titers were also inhibited by siMek1s. Also, the enhanced anti-viral effect can be seen in S08D compared with unmodified siRNA and S08L.

To determine the effects of siMek1s on cytopathic effect (CPE) of HSV-2 or EV71, HEK293 cells or RD cells transfected with siMek1s were infected with HSV-2 and EV71, and then monitored with phase-contrast microscopy every 12 h for 3 days p.i. In this experiment, mock infection, viral infection was used as controls. As shown in **Figure 4D**, at 24 h p.i., the cells transfected with 30 nM siMek1s were manifested much less CPE, as compared to virus and siMut1 controls. Of note, the S08D also show less CPE than others. The virus titer yielded in the supernatant further confirmed that D-IsoNA modification showed some potency-enhancing effect at passenger strand position 8 which could be applied in anti-HSV2 and EV71 therapy.

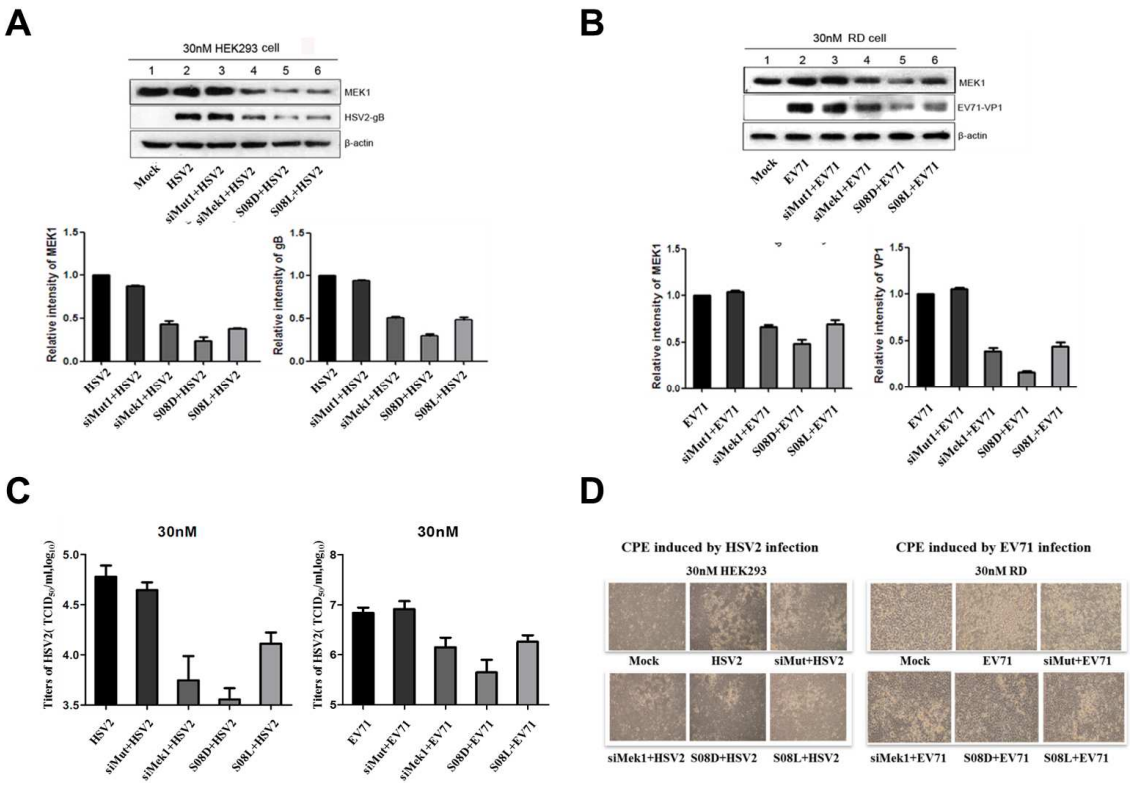

Figure 4. Anti-viral effects of D-/L-isoNA incorporation at position 8 and 9 of passenger strand. (A) and (B) Anti-HSV2 and anti-EV71 results of D-/L-modified siMek1s. The experiments were performed as described in Figure 1 except for virus infection with MOI of 1.5. Cell lysates collected at 24 p.i. were assayed for viral protein expressions by Western blot with monoclonal antibodies specific to HSV-2 gB protein or EV71 VP1 protein. Quantification of gB band and VP1 band were normalized by densitometric scanning of actin using the band leader software (version 3.0). The relative intensity of gB and VP1 on y-axis was presented by percentage of intensity of mock transfection (100%). The data were the average of three independent experiments and error bars denoted the standard deviations. (C) Viral titer of HSV2 and EV71 after incubation with D-/L-isoNA modified siMek1s. HEK 293 cells were infected with HSV-2 at an MOI of 1.5. The cells and medium were collected separately at different time points. Virus titers in the medium were measured by plaque assay. Data shown were the means±standard deviations (n = 3). The titers on y-axis represented logarithmic values. (D) CPE results with HSV2 and EV71 infection after incubation with D-/L-isoNA modified siMek1s. Cells were transfected with modified siRNAs 30nmol of each, and infected at 44 h post-transfection with 1.5 MOI of HSV-2. The effects of modified siRNAs on CPE were examined from 8 h p.i., and images were taken at 24 h p.i.

Discussion

Generally, during the process of RNA interference, the cleavage of passenger strand caused by Ago2 protein happens between nucleotide 9 and nucleotide 10. The chemical modifications and mismatches located at these two sites were able to interfere the cleavage process by disturbing the approach and interaction between cleavage related residues in Ago2-PAZ domain and the phosphodiester bond between nucleotide 9 and nucleotide 10. As a result, the silencing activity of modified siRNA would also be reduced.[11] In this report, we also found that no matter D-isoNA or L-isoNA was incorporated at position 9, the silencing efficiency of modified siRNA were reduced obviously, which is in consistent with other modification strategies. However, chemical modifications at other positions usually have no obvious influence on the cleavage process of passenger strand.[11] But we found that D-isoNA and L-isoNA modification next to the cleavage related site could also affect the cleavage process. Interestingly, D-isoNA and L-isoNA modification introduce quite opposite influence on the silencing efficiency when the modification happens at position 8 of passenger strand.

According to cleavage kinetics experiment, the passenger RNA strand with L-isoNA modification was cleaved much slower than unmodified passenger strand at the same position. Based on our previous reports,[18] L-isoNA modification may introduce dramatic regional conformation alteration not only at the incorporation site, but also around the incorporation

site. Therefore, when L-isoNA modification was placed next to the nucleotide 9, it would also disturb the tight interaction between the cleavage related residues and the corresponding phosphodiester bond. Although in the direct cleavage kinetics test, the passenger RNA strand with D-isoNA modification at position 8 showed no difference with unmodified passenger strand, they showed quite different influence on the vibration frequency of Ago2-PAZ domain in the molecular dynamic simulation. It may be also owing to the slight regional conformation alteration around the insert site caused by D-isoNA modification. However, the work about the precise mechanism for the enhanced vibration frequency of Ago2-PAZ domain is still ongoing. And, to the best of our knowledge, no modification strategy has enhanced the silencing activity by accelerating the movement frequency of PAZ domain. Although the degree of activity enhancement was not quite dramatic, it also provides us a more particular knowledge about the RNA interference process. Our work also reminds us that D-isoNA and L-isoNA, as a pair of chemical tools, could produce quite opposite influence on the interaction between protein and nucleotide, and they will be applied wildly in the mechanism studies in the future.

Experimental

Solid-phase synthesis of RNA oligonucleotides

RNA oligonucleotide synthesis was carried out on the 1 μmol scale using Applied Biosystems 394 DNA Synthesizer according to regular phosphoramidite chemistry. The 2'-OTBDMS protected D- and L-isoNA phosphoramidite monomers were synthesized as previously reported,[18] then the D-/L-isoNA phosphoramidite monomers were inserted singly into the siRNA sequence at the modified position targeting to MEK1 (**Figure 1B**). Furthermore, an extended coupling time of 900 second was used for D-/L-isoNA phosphoramidites instead of the standard coupling time of 600 second used for the four standard 2'-OTBDMS protected RNA phosphoramidites (A^{Bz}, C^{Ac}, G^{Ac} and U) due to the steric effect of isoNA phosphoramidites. Cleavage and deprotection of the oligomers were performed in concentrated ammonia at 55 °C for 24 h and TBDMS group was removed by treatment with Et_3N/HF in anhydrous DMSO. The crude product was purified by anion-exchange high-performance liquid chromatography (Dionex, DNAPac, PA200, 9×250mm) using a linear gradient of 12.5-40% eluent A in 40 min. Solutions of 0.02 M Tris-$HClO_4$ in 10% CH_3CN, pH = 8 was used as eluent B, and 0.4M $NaClO_4$ in eluent B was used as eluent A. Then, the purified oligonucleotides were desalted by Sephadex G25 column. The purity and identity of the oligonucleotides was confirmed by ion exchange chromatography and MOLDI-TOF MS, respectively, and all single strands were HPLC purified to >90% purity. Finally, the pure oligonucleotides were lyophilized and stored at -40 °C.

Antibodies

Antibodies were purchased from Cell Signaling Technology (anti-MEK1), East Coast Bio (anti-HSV gB monoclonal antibody), Abcam (polyclonal anti-EV71 VP1) and Santa Cruz Biotechnology (β-actin).

Cell culture

Rhabdomyosarcoma (RD) cells and Human embryonic kidney (HEK) 293 cells were grown in Dulbecco's modified Eagle's medium (DMEM, GIBCO) supplemented with 2% or 10% heat-inactivated fetal bovine serum (FBS, GIBCO) at 37 ^{o}C in a 5% CO_2 humidified incubator.

Virus infection

Monolayers of RD or HEK293 cells at 70–80% confluency were starved and infected with strain 333 of HSV-2 and wild type EV71 (EV71-BC08 stain) at various multiplicities of infection (MOI). After 1 h at 37 ◦C, the inoculum was removed and incubation continued in DMEM containing 2% FBS at 37◦C for viral growth. Supernatants collected at different time points post-infections (p.i.) were clarified by centrifugation (2000g), virus titers were determined by plaque assays carried out in triplicates. Virus was inactivated by being UV irradiated for 30 min using a Phillips TUV 30W bulb at a distance of 17 cm with occasional agitation, and then blind passaged for three generations to confirm loss of replicative capacity.

siRNA and transient transfection

For siRNA transfections, the INTERFERin reagent (Polyplus-transfection) was used according to the manufacturer's instructions. RD cells or HEK293 cells were grown in 12-well plates to 40% confluency. Cells were then transfected with 30 nM specific siRNAs and incubated for indicated hours, the medium was then replaced with DMEM containing with 1% FBS and cells starved for 8 h.

Morphological analysis

HEK 293 cells were examined following HSV-2 and EV71 infection at every 12h intervals post-infection for the cytopathic

effect (CPE) using phase-contrast microscopy.

Western blotting analysis

Cells were lysed in a buffer containing 20mM Hepes (pH 7.4), 100mM NaCl, 5mM EDTA (pH 7.4), 1mM Na_3VO_4, 30mM NaF, 5% glycerol, 0.1% SDS, 1% Triton X-100, 10mM p-nitrophenylphosphate, 1mM glycerophosphate, supplemented with complete protease inhibitors (Roche). Cell lysates were obtained by centrifugation at 4 ^{o}C, 13000 rpm and protein concentration was determined with the Bicinchoninic Acid Protein Assay Kit (Pierce). Proteins were resolved onto sodium dodecyl sulfate-polyacrylamide gel electrophoresis (SDS-PAGE), and transferred to PVDF membranes (Millipore). The membrane was blotted with specific primary antibodies, as indicated in figure legends, followed by incubation with secondary antibodies conjugated with horseradish peroxidase, and developed with an enhanced chemiluminescent substrate (ECL) or SuperSignal West Femto Maximum Sensitivity Substrate (Pierce).

Real-time quantitative PCR (Q-PCR)

Viral RNAs from supernatants were prepared using Trizol reagent (Invitrogen). Then, 1μg of total RNA was reverse transcribed into cDNA with the ReverAid First strand cDNA synthesis kit (Thermo Science). A quantitation standard curve was achieved using seven 10-fold serial dilutions of the recombinant plasmid standard DNA, which contained sequences derived from gB gene of HSV2 and VP1 gene of EV71, varying from $1x10^3$ to $1x10^9$ copies. Real-time quantitative (Q-PCR) was performed by targeting the gB gene and VP1 gene in 96-well plates with the Roche Light Cycler 480 system. Each 20 μL of reaction contained 10μL of 2x SYBR Green Supermix, 20 nM of target gene primer mix, and 20–50 ng of a cDNA template. The PCR reaction was set up as follows: initial denaturation step at 95 ^{o}C for 10 min, followed by 40 cycles of 30 s at 94 ^{o}C, at 55 ^{o}C for 30 s and at 72 ^{o}C for 30 s. Quantified results for the experimental samples were extrapolated from the standard curve, with all experimental samples being run in triplicate.

Molecular structures of Ago/siRNA complex

The eukaryotic Ago2 protein crystal structures were just reported,[4,5] while siRNA double helixes are not involved in the structures. For the highly structural similarity of the Ago family, Ago protein from *T. thermophiles* was used as a substitution. There are many *T. thermophiles* Ago proteins in the Protein Data Bank, such as 3HJF, 3HK2, 3HM9, 3HVR, 3HO1[23] and 3F73.[24] Ago protein from 3HVR was used, because there is no mutation and mismatch and there are two Mg^{2+} in the active site. The total nucleotides part from 3HK2 was used after the overlap of the Ago proteins in 3HVR and 3HK2, in which the RMSD of the same guide and target nucleotides (27nt) between 3HVR and 3HK2 is 1.54Å. Finally, some processes were carried out to make the siRNA available for the following molecular simulation, which includes changing the DNA-guide strand to RNA-guide strand, mutating the nucleotides sequence and modifying the specific nucleotide to isonucleotide according to **Figure 1B**. All the operation was performed in Discovery Studio 3.0.

Molecular dynamics simulation

All the molecular dynamics simulations were carried out with Amber 11 and the Amber 10 forcefield were used. The structures were solvated in a periodic truncated octahedral water box. The minimum distance between the complex and the box wall is 10Å. The TIP3P water model was applied and sodium ions were placed to neutralize the system. The Bonds linking hydrogen atoms were restrained by SHAKE algorithm. The Particle Mesh Ewald (PME) method was used to calculate the electrostatic interaction. The minimization of the systems consists of two stages, at first, respective 5000 steps of steepest descent and conjugate gradient were performed to avoid the contacts between waters by constraining the Ago/siRNA complex. Then the whole system was minimized under 5000 steps of steepest descent and conjugate gradient respectively. After the minimization of the solvated system, the general Heating-Equilibrium- Production pipeline was performed to each structure. The heating process was carried out for 20ps from 0K to 300K with 10kcal mol^{-1} $Å^{-2}$ harmonic constraint under NVT ensemble. The following equilibrium process lasted for 100ps when the harmonic constraint reduced to 0 gradually under NPT ensemble. Finally, 24ns production was conducted under NPT ensemble and the last 20ns trajectory was used for analyzing. The integration time step was 1fs, and the coordinate was saved every 10ps.

Principal component analysis

In order to observe the dominant motions of functional domains of Ago protein, principal component analysis (PCA)[25] was carried out using AmberTool 1.5. First, the coordinate covariance matrix of Ago protein was built up for each complex. Then the eigenvectors and eigenvalues of the covariance matrix were calculated by diagonalizing the matrix. The eigenvectors represent the collective motions of the Ago domains, while the corresponding eigenvalues suggest the importance of the motions. In this work the first three most important motions were picked up and projected to the trajectory. The extreme projection of each motion was used to indicate the directions of the functional domains.

MM/PBSA binding free energy calculation

The binding free energy between a ligand and a receptor is calculated by the following equation:

$$\Delta G_{b,s}=\Delta G_{b,v}+\Delta G_{s,c}-(\Delta G_{s,l}+\Delta G_{s,r})$$

$\Delta G_{b,s}$ and $\Delta G_{b,v}$ are the binding free energies in solution and vacuum, while $\Delta G_{s,c}$, $\Delta G_{s,l}$ and $\Delta G_{s,r}$ are the solvation free energy for the complex ,ligand and receptor. $\Delta G_{b,v}$ consists of interaction energy between ligand and receptor while sometimes entropy contribution is also under consideration. The solvation free energy is composed of electrostatic part and hydrophobic part. In this work the binding free energies of RISC/ssRNA for Ago/siRNA complexes are calculated using MM/PBSA method by MMPBSA.py module in AmberTool 1.5. For the differences within complexes are only the isonucleotides, the entropy contribution is neglected.

Acknowledgements

This work was supported by the Ministry of Science and Technology of China (Grant No. 2012AA022501, 2012CB720604, 2013CB966800), the National Natural Science Foundation of China (Grant No. 20932001).

Notes and references

1. A. Fire, S. Xu, M. K. Montgomery, S. A. Kostas, S. E. Driver and C. C. Mello, *Nature,* 1998, **391**, 806-811.
2. S. M. Elbashir, J. Harborth, W. Lendeckel, A. Yalcin, K. Weber and T. Tuschl, *Nature,* 2001, **411**, 494–498.
3. A. J. Hamilton and D. C. Baulcombe, *Science,* 1999, **286**, 950–952.
4. S. M. Elbashir, W. Lendeckel and T. Tuschl, *Genes Dev.,* 2001, **15**, 188–200.
5. P. D. Zamore, T. Tuschl, P. A. Sharp and D. P. Bartel, *Cell,* 2000, **101**, 25–33.
6. W. Filipowicz, *Cell,* 2005, **122**, 17-20.
7. H. W. Wang, C. Noland, B. Siridechadilok, D. W. Taylor, E. Ma, K. Felderer, J. A. Doudna and E. Nogales, *Nat. Struct. Mol. Biol.,* 2009*,* **16**, 1148-1153.
8. K. Miyoshi, H. Tsukumo, T. Nagami, H. Siomi and M. C. Siomi, *Genes Dev.,* 2005*,* **19**, 2837-2848.
9. K. Kim, Y. S. Lee and R. W. Carthew, *RNA,* 2007*,* **13**, 22-29.
10. X. Ye, N. Huang, Y. Liu, Z. Paroo, C. Huerta, P. Li, S. Chen, Q. Liu and H. Zhang, *Nat. Struct. Mol. Biol.,* 2001*,* **18**, 650-657.
11. P. J. Leuschner, S. L. Ameres, S. Kueng, and J. Martinez, *EMBO Rep.,* 2006*,* **7**, 314-320.
12. H. Addepalli, Meena, C. G. Peng, G. Wang, Y. Fan, K. Charisse, K. N. Jayaprakash, K. G. Rajeev, R. K. Pandey, G. Lavine, L. Zhang, K. Jahn-Hofmann, P. Hadwiger, M. Manoharan and M. A. Maier, *Nucleic Acids Res.,* 2010*,* **38**, 7320-7231.
13. H. W. Yu, L. R. Zhang, J. C. Zhou, L. T. Ma and L. H. Zhang, *Bioorg. Med. Chem.* 1996*,* **4**, 609-614.
14. H. Y. Zhang, X. J. Wu, H. W. Yu, L. T. Ma and L. H. Zhang, *Chinese Chemical Letts.* 1996*,* **12**, 1089-1090.
15. F. Wang, Y. Chen, Y. Huang, H. W. Jin, L. R. Zhang, Z. J. Yang and L. H. Zhang, *Sci. China Chem.,* 2012*,* **55**, 1−10.
16. Z. L. Wang, J. F. Shi, H. W. Jin, L. R. Zhang, J. F. Lu and L. H. Zhang, *Bioconjug. Chem.,* 2005, **16**, 1081−1087.
17. a. J. Zhang, Y. Chen, Y. Huang, H. W. Jin, R. P. Qiao, L. Xing, L. R. Zhang, Z. J. Yang and L. H. Zhang, *Org. Biomol. Chem.,* 2012*,* **10**, 7566-7577. b. Z. S. Li, R. P. Qiao, Q. Du, Z. J. Yang, L. R. Zhang, P. Z. Zhang, Z. C. Liang, and L. H. Zhang, *Bioconjug. Chem.*, 2007, **18** (4), 1017-1024.
18. Y. Huang, Z. Chen, Y. Chen, H. Zhang, Y. C. Zhang, Y. L. Zhao, Z. J. Yang, and L. H. Zhang, *Bioconjug. Chem.,* 2013*,* **24**, 951-959. 90.
19. L. Z. Yu, B. Xiong, W. X. Gao, C. M. Wang, Z. S. Zhong, L. J. Huo, Q. Wang, Y. Hou, K. Liu, X. J. Liu, H. Schatten, D. Y. Chen, and Q. Y. Sun, *Cell Cycle,* 2007*,* **6**, 330-338.
20. H. Zhang, H. Feng, L. Luo, Q. Zhou, Z. Luo and Y. Peng, *Virus Res.,* 2010*,* **150**, 22-27.
21. J. M. Steinbach, C. E. Weller, C. J. Booth and W. M. Saltzman, *J. Control. Release,* 2012, **162**, 102-110.
22. B. Premanand, T. K. Kiener, T. Meng, Y. R. Tan, Q. Jia, V. T. Chow and J. Kwang, *Antiviral Res.* 2012, **95**, 311-315.
23. Y. Wang, S. Juranek, H. Li, G. Sheng, G. S. Wardle, T. Tuschl and D. J. Patel, *Nature*, 2009, **461**, 754-761.
24. Y. Wang, S. Juranek, H. Li, G. Sheng, T. Tuschl and D. J. Patel *Nature,* 2008, **456**, 921-926.
25. A. Amadei, A. B. Linssen and H. J. Berendsen, *Proteins,* 1993, **17**, 412-425.